

# Photoluminescence Spectroscopy of Mass-Selected Electro sprayed Ions Embedded in Cryogenic Rare-Gas Matrixes

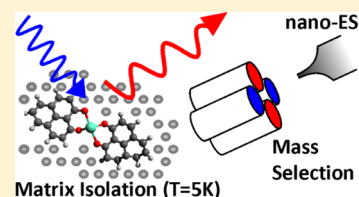
Bastian Kern,<sup>\*,†</sup> Jean-François Greisch,<sup>‡</sup> Dmitry Strelnikov,<sup>†</sup> Patrick Weis,<sup>†</sup> Artur Böttcher,<sup>†</sup> Mario Ruben,<sup>‡</sup> Bernhard Schäfer,<sup>‡</sup> Detlef Schooss,<sup>‡</sup> and Manfred M. Kappes<sup>\*,†,‡</sup>

<sup>†</sup>Institute of Physical Chemistry II, Karlsruhe Institute of Technology, Fritz-Haber-Weg 2, 76131 Karlsruhe, Germany

<sup>‡</sup>Institute of Nanotechnology, Karlsruhe Institute of Technology, Hermann-von-Helmholtz-Platz 1, 76344 Eggenstein-Leopoldshafen, Germany

## S Supporting Information

**ABSTRACT:** An apparatus is presented which combines nanoelectrospray ionization for isolation of large molecular ions from solution, mass-to-charge ratio selection in gas-phase, low-energy-ion-beam deposition into a (co-condensed) inert gas matrix and UV laser-induced visible-region photoluminescence (PL) of the matrix isolated ions. Performance is tested by depositing three different types of lanthanoid diketonate cations including also a dissociation product species not directly accessible by chemical synthesis. For these strongly photoluminescent ions, accumulation of some femto- to picomoles in a neon matrix (over a time scale of tens of minutes to several hours) is sufficient to obtain well-resolved dispersed emission spectra. We have ruled out contributions to these spectra due to charge neutralization or fragmentation during deposition by also acquiring photoluminescence spectra of the same ionic species in the gas phase.



Electrospray ionization (ESI) is a soft, generally applicable ionization technique which allows large complex molecules to be transferred from solution into the gas phase.<sup>1</sup> ESI, and in particular the nano-ESI variant of the technique, which uses nanoliter sample sizes, are therefore mainstays of modern analytical mass spectrometry. ESI has also been used to generate ion beams for “soft-landing” experiments in which mass-selected ions are deposited onto surfaces at impact energies of typically <math><0.1\text{ eV/atom}</math> so as to preclude significant impact-induced fragmentation.<sup>2</sup> In particular ESI-deposition under (ultra-) high vacuum conditions has been extensively used to decorate clean metal single crystal or silicon wafer surfaces with submonolayer coverages of many different kinds of molecules and molecular aggregates, for detailed structural probes using (low-temperature) STM. The systems studied have included organic fluorophores,<sup>3</sup> proteins,<sup>4</sup> DNA strands,<sup>5</sup> metallorganic complexes,<sup>6–9</sup> and metalloporphyrin supramolecular assemblies.<sup>10</sup> Although there has recently been significant progress in raising ion currents in prototype setups,<sup>11</sup> most deposition studies have made use of ESI and nano-ESI sources originally developed for analytical mass spectrometry. It is hard to achieve significantly more than several hundred picoamps of mass-selected ion currents at the deposition targets with such “analytical” ESI sources. By comparison, other more specialized molecular ion sources such as electron impact (e.g., for sublimed fullerenes<sup>12</sup> or polyaromatic hydrocarbons<sup>13</sup>) easily reach more than 100 nA of mass-selected ion currents, thus accessing a “preparative mass spectrometry” regime for materials research which is presently still beyond the horizon for ESI. Nevertheless, ESI deposition can already be routinely used to create ensembles of  $>10^{12}$  mass-selected molecules for spectroscopy. Here we

report an apparatus which realizes nano-ESI deposition into a cryogenic inert gas matrix for high-sensitivity photoluminescence spectroscopy. Whereas mass-selected ion deposition into an inert gas matrix is already a well-established method which has yielded absorption and photoluminescence spectra of numerous matrix-isolated molecular ions,<sup>14</sup> nano-ESI has not previously been adapted for this purpose. One application of this is to unravel the optical properties of solutions of multimetal inorganic complexes comprising several spectrally overlapping chromophores (e.g., in different oxidation states), by electro spraying, mass-selecting, depositing, accumulating, and then spectroscopically characterizing the components. At the same time, varying the matrix composition allows one to systematically probe environmental interactions on the dispersed ions.

## EXPERIMENTAL SECTION

**Overview.** Figure 1 presents a schematic of the UHV-compatible apparatus. It combines a home-built nanoelectrospray ion source (nano-ESI), with a quadrupole filter mass-selection stage and a deposition chamber for soft-landing of ions onto a substrate held at  $\sim 5\text{ K}$ . Ions are codeposited with an excess of an inert gas, typically neon, to form a cryogenic inert gas matrix for matrix isolation spectroscopy of the embedded species.<sup>15</sup>

**Nano-ES Ion Source.** Solutions containing the species of interest were filled into borosilicate glass nano-ESI needles which terminated in tips of approximately  $1\text{--}2\ \mu\text{m}$  inner

Received: September 14, 2015

Accepted: November 10, 2015

Published: November 10, 2015

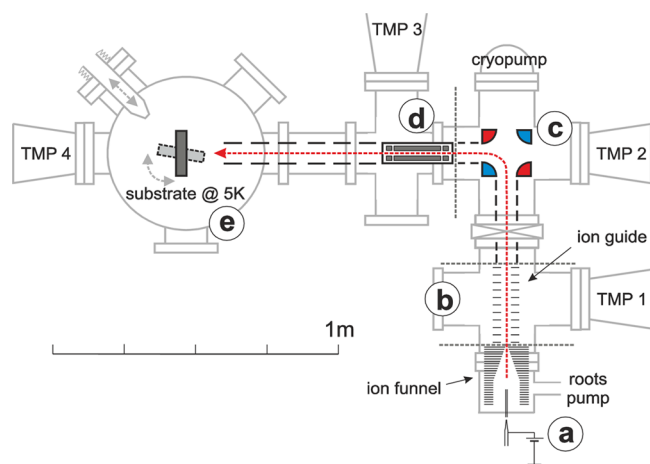


**Figure 1.** Schematic overview of the nano-electrospray ionization and matrix isolation experiment, (a) nano-ESI source at ambient pressure, (b) radio frequency ion funnel ( $p = 4 \times 10^{-1}$  mbar) and radio frequency ion guide ( $p = 1 \times 10^{-5}$  mbar), (c) electrostatic quadrupole deflector for separation of neutrals from ions, (d) quadrupole mass filter, (e) deposition chamber with gas inlet and cold substrate ( $T \sim 5$  K;  $p = 5 \times 10^{-8}$  mbar without matrix gas codeposition,  $p = 1 \times 10^{-5}$  mbar with matrix gas). Gray lines mark the different vacuum stages.

diameter Typical sample volumes were  $30 \mu\text{L}$  which proved sufficient for approximately 12 h of operation. Filled nano-ESI needles were positioned about 2 mm away from the entrance of the desolvation capillary leading into the first vacuum stage of the nano-ESI source. To reduce the flow of solvent vapor into the first vacuum chamber, the desolvation capillary was aligned slightly off the ion beam axis by approximately  $4^\circ$ . Electro-spraying was initiated by applying a voltage of 5–14 kV (in positive or negative mode) to the nano-ESI needle, relative to the entrance of the desolvation capillary. The desolvation capillary was composed of stainless steel and had a length 100 mm, had an i.d. of 0.5 mm, and was held at  $T = 150^\circ\text{C}$ .

**Ion Optics.** Following transit through the desolvation capillary into the first vacuum stage, ions were collisionally/electrostatically focused using a home-built rf ion funnel,<sup>16</sup> thus enhancing ion transmission into the downstream regions of the instrument. The ion funnel is composed of a series of 73 ring electrodes (0.5 mm thick stainless steel plates), forming a 27 mm drift region and a 45 mm focusing region with progressively decreasing inner diameters (from 25 mm to 3 mm). The electrodes were separated by Teflon sheets (0.5 mm thick). The ion funnel “empties” into an rf ion guide consisting of 43 ring electrodes, with a constant inner diameter of 8 mm. The electrodes are evenly spaced over a total length of 140 mm, separated by 2.8 mm Viton spacers to allow for differential pumping by TMP 1 (see Figure 1). To provide the dc potential gradient ( $\sim 130$  V over the total length), adjacent electrodes of the funnel and the ion guide are connected by  $1 \text{ M}\Omega$  resistors. Each electrode is also connected to one of the two alternating outputs of a home-built rf power supply (500 kHz, amplitude 330 V) with a 200 pF capacitor which ensures that the phase difference between adjacent electrodes is  $180^\circ$ .

Ions emanating from the rf ion guide were then transferred through cylindrical electrostatic Einzel lenses to an electrostatic quadrupole deflector which deflects charged particles by 90 deg but allows neutral molecules to continue straight on the axis unaffected, thus preventing contamination of the cryomatrix sample by residual neutrals from the ion source. The deflected

ions were focused into a quadrupole mass filter (QMS; Extrel) to select the desired mass-to-charge ratio, thereby removing unwanted charged species such as adducts with solvent molecules. For the experiments reported here, we used a QMS with 19 mm rods equipped with a pre- and postfilter assembly. This was driven by a 880 kHz power supply which allowed for a mass range of up to  $m/z = 1000$  amu/e in mass resolving mode. To keep deposition times manageable, the mass resolution was typically tuned down to  $m/\Delta m \sim 30$ , which ensures high ion transmission while providing enough mass resolution to separate solvent adduct species from their parent ions. Mass resolving mode was used for deposition of  $\text{Gd}(\text{PLN})_2^+$  (see the Supporting Information for a typical mass scan). However, the molecular masses of both  $[\text{Gd}_9(\text{PLN})_{16}(\text{OH})_{10}]^+$  and  $[\text{Eu}_9(\text{PLN})_{16}(\text{OH})_{10}]^+$  were beyond the mass filter range. Consequently for deposition of  $[\text{Gd}_9(\text{PLN})_{16}(\text{OH})_{10}]^+$  and  $[\text{Eu}_9(\text{PLN})_{16}(\text{OH})_{10}]^+$ , the QMS was run in rf-only mode with its low mass cutoff set near  $m/z = 1000$  amu/e, thus acting as a high pass filter for heavy ions. Using a comparable nano-ESI source run under the same conditions and interfaced with a higher mass range analytical mass spectrometer, we had previously ascertained that both species are by far (>95% integrated intensity) the dominant ionic species obtained by ESI of the respective pure solutions.<sup>17</sup>

Following the QMS, several Einzel lenses focused the ion beam onto the cold ( $T \sim 5$  K) target. Prior to the deposition, the ion current can be monitored with a picoammeter (Keithley, model 6485). All voltages and currents can be adjusted and tracked electronically within LabView (National Instruments). The total ion current of the nano-ESI source was measured to be approximately 5 nA under typical conditions. The mass selected ion current depends strongly on the species sprayed and can reach 300 pA after mass selection, which corresponds to a maximum transmission of 6% through the entire ion optical setup from nano-ESI source to target.

**Vacuum Setup.** Electroprayed ions are transferred from ambient pressure to the deposition target through four differentially pumped vacuum stages. The first two stages (located in the chamber (b), see Figure 1) comprise the rf funnel and subsequent ion transfer regions with operating pressures of  $p_{\text{first}} \sim 4 \times 10^{-1}$  mbar and  $p_{\text{second}} \sim 1 \times 10^{-5}$  mbar. They are pumped by a  $505 \text{ m}^3/\text{h}$  Roots blower and  $680 \text{ L s}^{-1}$  turbomolecular pump (TMP1), respectively. The vacuum chamber (b) can be decoupled from the rest of the apparatus by means of a gate valve when no ion deposition is being performed. This keeps the contamination gas load at the deposition target to a minimum. The electrostatic deflector is located in the third differential pumping stage which is evacuated by a combination of a  $500 \text{ L s}^{-1}$  turbomolecular pump (TMP2) and a cryopump (Figure 1c) to a typical operating pressure of  $\sim 1 \times 10^{-7}$  mbar. The cryopump ( $\sim 2000 \text{ L s}^{-1}$ ) is positioned behind the deflector on the primary beam axis, i.e., in direct line of sight with the nano-ESI source. This ensures that residual solvent molecules are efficiently trapped and do not diffuse into the deposition chamber. The quadrupole mass filter is located between the third (TMP3) and the endmost (fourth, TMP4) pumping stages (Figure 1e). Its housing acts as an aperture for differential pumping (Figure 1d). The base pressure in the deposition chamber (pumped by two turbomolecular pumps, 70 and  $690 \text{ L s}^{-1}$ , respectively) was below  $1 \times 10^{-8}$  mbar with the nano-ESI source region connected. During matrix gas codeposition, this pressure rose to  $\sim 10^{-5}$  mbar. A load-lock chamber attached to the deposition

chamber allows changing the substrate without breaking vacuum.

**Sample Preparation.** To prepare samples of matrix isolated ions for spectroscopy, the ion beam was codeposited at a nominal kinetic energy of <50 eV together with an excess of matrix gas onto a cold aluminum coated sapphire substrate cooled to  $\sim 5$  K by a closed-cycle helium cryostat (SHI Cryogenic, RDK-415D). An operating temperature of  $\sim 5$  K enables the use of neon as matrix gas which is optimally suited for matrix isolation photoluminescence spectroscopy.<sup>15</sup> The ion current directed at the substrate was between 10 pA and 300 pA (i.e., between  $6 \times 10^7$  and  $1.9 \times 10^9$  singly charged ions per second), depending on the species to be deposited. Our UHV compatible apparatus ensures comparatively clean deposition conditions with little solvent or background gas contamination of the resulting matrixes. Consequently ionic species can be deposited over long time scales (up to days) without appreciable sample degradation. For the experiments reported below, the total amount of ions deposited into a spot of  $\sim 1$  cm diameter was typically  $10^{12}$  to  $10^{13}$  at a ratio of matrix to guest molecule of about  $5 \times 10^5:1$ , effectively isolating the deposited ions from each other. The thickness of the corresponding matrixes was approximated based on overall neon dose (determined from exposure time and neon pressure at the corresponding pumping speed) which was calibrated against interference fringes measured for analogous neon matrixes using an infrared absorption spectrometer.<sup>18</sup> In the experiments reported here, neon matrix thickness ranged from 1 to 20  $\mu\text{m}$ .

**Charge-States in Matrix.** When depositing ionic species of only one polarity into an insulating matrix, charge accumulates. Eventually it must be (partially) compensated, otherwise further incoming ions start to be deflected thus limiting the amount collected.<sup>2,19</sup> This can be accomplished by introducing counterions into the matrix, e.g., by capture of electrons drawn into the (positively charged) matrix from nearby low work function surfaces. In the simplest variant of this, deposited cations can make their own counteranions by way of multiple electron capture steps. For example, we have recently shown that  $\text{C}_{60}^+$  deposited into neon can become neutralized and further converted to  $\text{C}_{60}^-$  while close to the matrix surface.<sup>13</sup> More commonly, counteranions can be generated by electron attachment to (neutral) impurities already present in the matrix or by attachment to intentionally doped electron scavengers like  $\text{CCl}_4$  or  $\text{CO}_2$  (clusters). In the present work we have followed this approach, not only to ensure the highest cation loadings but also to restrict neutralization. Specifically, we have compared the photoluminescence spectra of matrix-isolated species prepared by depositing mass-selected ions into pure Ne, Ne + 0.1%  $\text{CO}_2$ , Ne + 0.3%  $\text{CO}_2$ , Ne + 0.7%  $\text{CO}_2$ , and Ne + 0.01%  $\text{CCl}_4$ .

**Photoluminescence Measurements in Matrix.** Following preparation, matrix-isolated samples were rotated by  $80^\circ$  in the plane of the apparatus (while maintaining sample temperature and chamber pressure) to allow for photoluminescence spectroscopy, see Figure 1. In the experiments reported here, substrates were then irradiated with a partially focused 375 nm CW diode laser (Thorlabs, 20 mW, 1 nm bandwidth). The irradiated area was  $\sim 1$  mm<sup>2</sup>, i.e., only 1–2% of the deposited ions were probed. The emitted light was collected using a focusing lens ( $d = 1.4$  cm; focal length 10 mm) positioned about 50 mm from the surface and then transferred through a fiber-optic bundle to a spectrometer. We estimate the collection efficiency for emitted light to be roughly

1%. Two different spectrometers were used depending on photoluminescence signal intensities: an ARC SpectraPro-500 spectrograph equipped with an EG&G PARC 1456A detector or a Princeton Instruments IsoPlane SCT320 spectrograph with a PIXIS 256 OE camera (spectral range for both setups, 200–1100 nm). In both cases we employed entrance aperture slits of 50  $\mu\text{m}$ . The corresponding spectral resolutions were 0.3 and 0.12 nm, respectively. The acquisition time per spectrum reported ranged from 300 to 2400 s.

**Photoluminescence in Gas-Phase.** Below we compare matrix measurements with photoluminescence spectra of the same ions in gas-phase. The apparatus used to measure trapped ion photoluminescence spectra has been described elsewhere.<sup>20</sup> The  $[\text{Eu}_9(\text{PLN})_{16}(\text{OH})_{10}]^+$  spectrum was obtained as reported in ref 17. Briefly, the ions were prepared using an identical nano-ES ion source, mass-selected, and then injected into an electrostatic Paul ion trap held at  $\sim 83$  K. They were stored in the trap operated at 300 kHz under a pressure of 0.2 mbar helium on time scales of seconds (50 measurement cycles of 50s each), each bunch of ions was irradiated for 20 s at an irradiance of 55 W/cm<sup>2</sup> for  $[\text{Eu}_9(\text{PLN})_{16}(\text{OH})_{10}]^+$  and 1975 W/cm<sup>2</sup> for  $[\text{Gd}_9(\text{PLN})_{16}(\text{OH})_{10}]^+$  using the 476.5 nm line of an argon-ion laser (laser model 2080-15S, Spectra-Physics). The dispersed photoluminescence spectra were recorded using a monochromator (Triax 190, Jobin Yvon Horiba)/CCD (Newton EMCCD A-DU-970N-BV, Andor) combination with a spectral resolution of 2.4 nm (300 grooves/mm grating) or 0.5 nm (1200 grooves/mm (“high resolution”). In the case of the strongly photoluminescent  $\text{Gd}(\text{PLN})_2^+$  ions used in the present work to compare the sensitivity of both setups, the gas-phase spectrum shown in Figure 2c was acquired for samples of

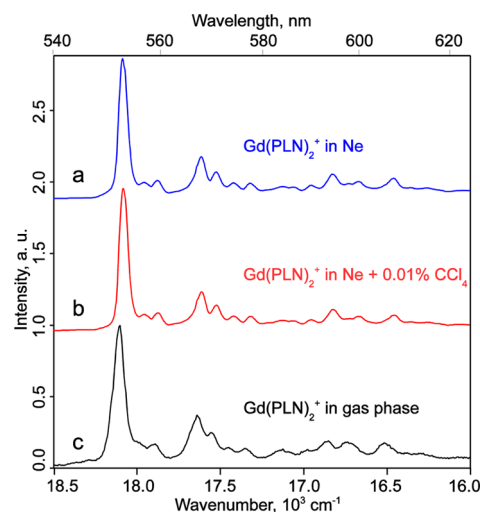


**Figure 2.** Photoluminescence spectra of  $\text{Gd}(\text{PLN})_2^+$ : (a) after deposition into a pure neon matrix at 5 K (375 nm excitation), (b) in a Ne + 0.01%  $\text{CCl}_4$  matrix at 5 K (375 nm excitation), and (c) in the gas phase at 83 K (458 nm excitation). Whereas the matrix, spectra in parts a and b are identical, the gas-phase measurement is slightly blue-shifted (see text for details).

$\sim 10^5$  mass-selected ions stored at  $\sim 83$  K under a helium pressure of 0.2 mbar in a trap operated at 600 kHz using the 458 nm line of an argon-ion laser (laser model 2080-15S, Spectra-Physics) and an irradiance of 375 W/cm<sup>2</sup>. The spectrum shown was recorded over  $100 \times 60$  s excitation periods with one period per cycle. Note that the number of ions

stored in the TLIF trap at a given time is limited to  $\sim 10^5$  ions due to space charge effects. In order to prevent as well as monitor photodissociation, the TLIF experiment is run in measurement cycles comprising ion injection into the trap, mass-selection, thermalization, photoluminescence acquisition, ion ejection coupled to mass analysis, and refilling. Each cycle takes between 50 s ( $[\text{Eu}_9(\text{PLN})_{16}(\text{OH})_{10}]^+$ ) and 90 s ( $\text{Gd}(\text{PLN})_2^+$ ).

## RESULTS AND DISCUSSION

To demonstrate the potential of the nano-ESI-deposition setup, several proof-of-principle measurements were carried out with test systems chosen to cover a range of different masses and luminescence properties. Specifically, three rare-earth complexes with strongly absorbing phenalen-1-one (PLN) ligands<sup>17</sup> were deposited, namely,  $\text{Gd}(\text{PLN})_2^+$ ,  $[\text{Gd}_9(\text{PLN})_{16}(\text{OH})_{10}]^+$ , and  $[\text{Eu}_9(\text{PLN})_{16}(\text{OH})_{10}]^+$ . To first order, these species can be regarded as purely ionic complexes comprising singly negatively charged PLN ligands and 3-fold positively charged lanthanoid cations, thus yielding “composite” ions with an overall charge of +1.

We have previously reported the gas-phase photoluminescence spectra of  $[\text{Gd}_9(\text{PLN})_{16}(\text{OH})_{10}]^+$  and  $[\text{Eu}_9(\text{PLN})_{16}(\text{OH})_{10}]^+$ .<sup>16</sup>  $\text{Gd}(\text{PLN})_2^+$  has not been previously studied, neither in the matrix nor in the gas-phase.

**$\text{Gd}(\text{PLN})_2^+$ .**  $\text{Gd}(\text{PLN})_2^+$  containing ion beams was obtained by nano-ESI of DMSO solutions of  $\text{Gd}(\text{PLN})_4\text{Na}$ , synthesized as described in ref 21.  $\text{Gd}(\text{PLN})_2^+$  is coordinatively unsaturated and is likely mainly formed during nano-ESI via the elimination of coordinating solvent molecules.  $[\text{Gd}_9(\text{PLN})_{16}(\text{OH})_{10}]^+$  and  $[\text{Eu}_9(\text{PLN})_{16}(\text{OH})_{10}]^+$  ion beams were prepared as described in ref 17 and sprayed from DCM.

$\text{Gd}(\text{PLN})_2^+$  spectra in pure neon matrix exhibit sharp, vibronically resolved features with the strongest emission line around  $18\,090\text{ cm}^{-1}$ , Figure 2a. We assign these to  $T_1 \rightarrow S_0$  phosphorescence of the PLN ligand.<sup>22</sup> We observed no further emission features. In particular, we saw neither PLN  $S_1 \rightarrow S_0$  fluorescence nor, as expected, emission from gadolinium metal centers. Apparently, intersystem crossing from the  $S_1$  state (populated by 375/458 nm absorption) to the emitting  $T_1$  state is very efficient. To exclude spectral contributions from another projectile-ion-derived charge state, e.g., as a result of neutralization during deposition, we also codeposited  $\text{Gd}(\text{PLN})_2^+$  together with a mixture of Ne + 0.01%  $\text{CCl}_4$  (Figure 2b). These electron scavenger doped matrixes are expected to have a lower propensity for neutralization of the incident cations. The corresponding photoluminescence spectra show no changes in relative intensities of emission lines compared to the pure Ne measurement, suggesting that the only emitting charge state present in the matrix is the incident cation.

This inference was confirmed by comparing the matrix spectra to the dispersed photoluminescence of  $\text{Gd}(\text{PLN})_2^+$  in gas phase (Figure 2c;  $10^5$  ions in 0.2 mbar helium; details to be reported elsewhere). While the position and shape of the phosphorescence emission features are weakly affected by the low temperature solid neon environment (Figure 2a,b) with red shifts ranging from 20 to  $55\text{ cm}^{-1}$ , the overall spectral pattern is essentially identical. Ab initio calculations of the ground state structure and excited state properties of  $\text{Gd}(\text{PLN})_2^+$  will be reported on in a future publication.<sup>23</sup>

To illustrate the potential of the matrix deposition method for enhancing signals of weakly emitting luminophore ions by accumulating them over long times, increasing amounts of

$\text{Gd}(\text{PLN})_2^+$  were deposited at a constant dilution ratio ( $1:10^5$ ) for a total duration of 22.75 h. At various times during this procedure, we recorded the corresponding photoluminescence spectra under otherwise identical conditions (375 nm/20 mW irradiation, 10 s acquisition (Figure 3)). The integrated

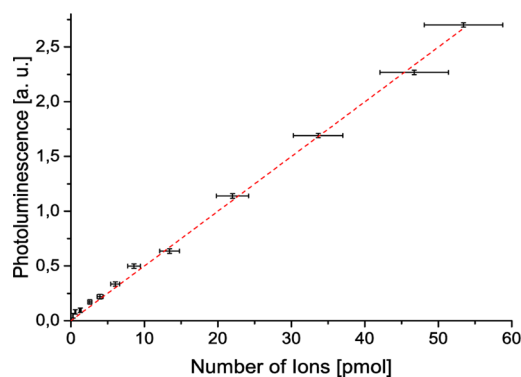


**Figure 3.** Integral photoluminescence of  $\text{Gd}(\text{PLN})_2^+$  as measured over the band origin at  $18\,090\text{ cm}^{-1}$  for various numbers of deposited ions embedded in neon at constant dilution ratio of about  $1:10^5$ . The integral photoluminescence increases linearly with the number of deposited ions (linear regression  $R^2 = 0.998$ ). The deposition time corresponding to 53.4 pmol was 22.75 h.

emission intensity clearly increases linearly with the number of deposited ions. No saturation of the signal occurs. Also, no signal degradation is detected upon irradiation. A further increase of the signal is possible by increasing the photoluminescence acquisition time or the irradiance.

**$[\text{Gd}_9(\text{PLN})_{16}(\text{OH})_{10}]^+$ .**  $[\text{Gd}_9(\text{PLN})_{16}(\text{OH})_{10}]^+$  in neon matrix (Figure 4a) shows a very broad ( $900\text{ cm}^{-1}$  bandwidth) emission feature, centered at  $17\,200\text{ cm}^{-1}$  with two shoulders at  $16\,000$  and  $14\,700\text{ cm}^{-1}$ . Overall, the observed emission band can again be assigned to  $T_1 \rightarrow S_0$  phosphorescence of the PLN ligands. However, unlike the sharp vibronic emission features of the  $\text{Gd}(\text{PLN})_2^+$  complex, this phosphorescence is strongly

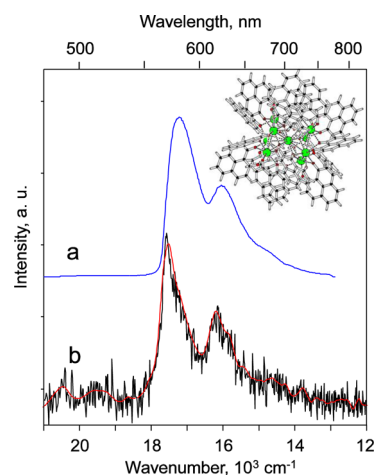


**Figure 4.** Photoluminescence spectra of  $[\text{Gd}_9(\text{PLN})_{16}(\text{OH})_{10}]^+$ : (a) after deposition into a pure neon matrix at 5 K (375 nm excitation wavelength) and (b) in the gas phase at 83 K (476.5 nm excitation wavelength),<sup>16</sup> in red, the corresponding smoothed spectrum low pass FFT filter). Shown in the inset is a representation of the molecular structure of  $[\text{Gd}_9(\text{PLN})_{16}(\text{OH})_{10}]^+$  with external PLN “antennas” adjacent to the neon matrix and an internal  $\text{Gd}^{3+}$  cluster core.

broadened even at 5 K. There are two symmetry inequivalent PLNs in the isolated molecule<sup>17</sup> so that inhomogeneous broadening seems unlikely to be the main reason for the comparatively featureless emission. Conceivably, stacking interactions between pairs or clusters of PLN ligands are responsible.<sup>24</sup>

In the case of matrix-isolated  $[\text{Eu}_9(\text{PLN})_{16}(\text{OH})_{10}]^+$  (Figure 5a), the photoluminescence spectrum shows very clear

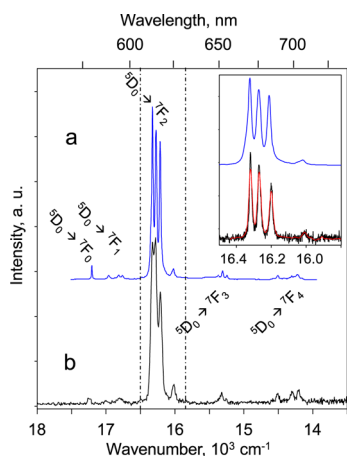


**Figure 5.** Photoluminescence spectra of  $[\text{Eu}_9(\text{PLN})_{16}(\text{OH})_{10}]^+$ : (a) deposited into pure neon matrix at 5 K (375 nm excitation wavelength) and (b) in gas phase at 83 K (476.5 nm excitation wavelength).<sup>17</sup> The insets contrast an expanded scale view of the matrix measurement (blue) with a separate high-resolution gas-phase measurement (black, smoothed in red).

emission features corresponding to  $\text{Eu}^{3+}$  transitions<sup>25</sup> ( $^5\text{D}_0 \rightarrow ^7\text{F}_0$  (17 180  $\text{cm}^{-1}$ ),  $^5\text{D}_0 \rightarrow ^7\text{F}_1$  (16 740–16 950  $\text{cm}^{-1}$ ),  $^5\text{D}_0 \rightarrow ^7\text{F}_2$  (15 950–16 400  $\text{cm}^{-1}$ ),  $^5\text{D}_0 \rightarrow ^7\text{F}_3$  (15 200–15 400  $\text{cm}^{-1}$ ), and  $^5\text{D}_0 \rightarrow ^7\text{F}_4$  (14 100–14 600  $\text{cm}^{-1}$ )). These are dominated by the hypersensitive  $^5\text{D}_0 \rightarrow ^7\text{F}_2$  band. In contrast to the structurally analogous  $[\text{Gd}_9(\text{PLN})_{16}(\text{OH})_{10}]^+$  (see insert in Figure 4), matrix isolated  $[\text{Eu}_9(\text{PLN})_{16}(\text{OH})_{10}]^+$  shows no measurable PLN emission. This reflects very efficient resonant energy transfer from the  $\text{T}_1$  state of the PLN ligands (transiently populated by ISC from initially photoexcited  $\text{S}_1$  states) to energetically close-lying  $\text{Eu}^{3+}$  levels.<sup>17</sup> In contrast, such energy transfer is not possible for  $\text{Gd}^{3+}$  which has no excited states in the right energy range.

When comparing the matrix spectra for deposited  $[\text{Gd}_9(\text{PLN})_{16}(\text{OH})_{10}]^+$  and  $[\text{Eu}_9(\text{PLN})_{16}(\text{OH})_{10}]^+$  with the corresponding gas phase measurements<sup>17</sup> (Figure 4b and Figure 5b), we first note the remarkable agreement between the respective data sets. This supports our assignment of the matrix spectra to the as-deposited cations. Apparently, reduction and fragmentation (e.g., PLN<sup>-</sup> loss) during deposition do not yield significant amounts of species with photoluminescence properties clearly distinguishable from those of the incident ions. A closer inspection of the  $[\text{Gd}_9(\text{PLN})_{16}(\text{OH})_{10}]^+$  matrix spectrum reveals a modest  $\sim 400 \text{ cm}^{-1}$  red-shift of the PLN phosphorescence maximum compared to the gas-phase. In contrast, the  $\text{Eu}^{3+}$  emission features seen upon photoexcitation of  $[\text{Eu}_9(\text{PLN})_{16}(\text{OH})_{10}]^+$  are essentially unaffected by the neon matrix. The corresponding red-shifts are never more than  $30 \text{ cm}^{-1}$ . Apparently, the well-shielded f-electrons of the  $\text{Eu}^{3+}$  centers of the  $[\text{Eu}_9(\text{PLN})_{16}(\text{OH})_{10}]^+$  ions are only weakly influenced by the dielectric environment of the PLN antennas.

## CONCLUSIONS

A combination of nano-ESI, mass-to-charge selection, soft-landing into codeposited cryogenic inert gas matrix, and photoluminescence spectroscopy has been demonstrated and used to analyze the optical properties of various strongly emitting electrosprayed test systems. Such low energy ion deposition into an insulating matrix can sometimes be associated with significant neutralization and fragmentation, thus complicating the assignment of observed spectral features. We have used two different strategies to ameliorate this issue: (i) doping of the co-condensed matrix with neutral electron scavengers during ion deposition so as to reduce neutralization of the ions of interest (i.e., to intentionally change the resulting charge state ratios) and (ii) comparison of matrix measurements with gas-phase measurements of the same ions under rigorously mass- and charge-specific conditions.

Specifically, we have deposited the lanthanoid complexes  $\text{Gd}(\text{PLN})_2^+$ ,  $[\text{Gd}_9(\text{PLN})_{16}(\text{OH})_{10}]^+$ , and  $[\text{Eu}_9(\text{PLN})_{16}(\text{OH})_{10}]^+$  as test systems. Each of these shows characteristic emission features in the neon matrix at 5 K when excited at 375 nm. We assign these emission features to the photoluminescence of the deposited ions by comparison to measurements of the same species in gas phase at 83 K. Interaction with the neon matrix induces only modest red shifts of the vibronically resolved PLN phosphorescence of  $\text{Gd}(\text{PLN})_2^+$ , whereas the broadened PLN phosphorescence of the larger  $[\text{Gd}_9(\text{PLN})_{16}(\text{OH})_{10}]^+$  is red-shifted by  $400 \text{ cm}^{-1}$ . By contrast, in the structurally analogous  $[\text{Eu}_9(\text{PLN})_{16}(\text{OH})_{10}]^+$ , photoexcitation of the antenna is associated with resonant energy transfer to  $\text{Eu}^{3+}$  centers. The resulting  $\text{Eu}^{3+}$  emission is practically unaffected by insertion into a neon matrix. We conclude that the solid neon environment induces very little geometric and electronic perturbation of the test species studied.

Neither the energetic position nor the relative intensities of the photoluminescence features recorded for each of the three test systems is changed by addition of the electron scavenger  $\text{CCl}_4$  to the neon matrix during ion deposition. We conclude that no other molecular charge states (or fragments) contribute to the spectra. Note that the emission features recorded at 5 K in the neon matrix and at 83 K in the gas-phase (in a 0.2 mbar helium atmosphere) have comparable bandwidths. Apparently, inhomogeneous broadening due to multiple matrix sites is compensated by the lower temperature and more effective thermalization.

Our new apparatus opens the possibility of accumulating deposited ions in matrix over long time periods (up to several days), thus also allowing measurements of very weakly photoluminescent systems. In particular, it is possible to characterize species which do not luminesce strongly enough to allow gas-phase measurements. A detailed account of the properties of a homologous series of luminescent lanthanide diketonate cations ( $\text{Ln}(\text{PLN})_2^+$ ,  $\text{Ln} = \text{Pr}, \text{Eu}, \text{Gd}, \text{Tb}, \text{Dy}, \text{Yb}$ , and  $\text{Lu}$ ), including also several systems which can only be measured in neon matrix, will be given in a subsequent paper.

The present apparatus performance could be further improved by implementing a more intense (larger capillary diameter or multicapillary) nano-ESI source. Better overlap between excitation laser and ion beam spots can be achieved by focusing the ions without significant broadening of their kinetic energy distribution, e.g., by using a planar ion funnel.<sup>26</sup> Also, the light collection efficiency of the setup could be enhanced by

a factor of 2–3 with only modest effort. Finally, simultaneous deposition of equal currents of (ESI-sprayed) anions and cations offers the hope of higher loadings of the selected charge states.<sup>27</sup> Given such improvements, one can envisage coupling of mass- and ion mobility preselection<sup>28</sup> so as to fractionate also by collision cross section prior to soft-landing. This would allow for conformer-/isomer-specific photoluminescence measurements of matrix isolated species.

## ■ ASSOCIATED CONTENT

### ● Supporting Information

The Supporting Information is available free of charge on the ACS Publications website at DOI: [10.1021/acs.analchem.5b03491](https://doi.org/10.1021/acs.analchem.5b03491).

Partial mass spectrum of Gd(PLN)<sub>4</sub>Na electrosprayed from DMSO solution (PDF)

## ■ AUTHOR INFORMATION

### Corresponding Authors

\*E-mail: [bastian.kern@kit.edu](mailto:bastian.kern@kit.edu). Fax: +49 721 608–47232.

\*E-mail: [manfred.kappes@kit.edu](mailto:manfred.kappes@kit.edu).

### Notes

The authors declare no competing financial interest.

## ■ ACKNOWLEDGMENTS

This work was supported by the Deutsche Forschungsgemeinschaft (DFG) through Subprojects C5, C6 and C7 of the Transregio Sonderforschungsbereich TRR 88 (“3MET”).

## ■ REFERENCES

- (1) Fenn, J. B.; Mann, M.; Meng, C. K.; Wong, S. F.; Whitehouse, C. M. *Science* **1989**, *246*, 64–71.
- (2) Laskin, J.; Wang, P.; Hadjar, O. *Phys. Chem. Chem. Phys.* **2008**, *10*, 1079–1090.
- (3) Rauschenbach, S.; Vogelgesang, R.; Malinowski, N.; Gerlach, J. W.; Benyoucef, M.; Costantini, G.; Deng, Z.; Thontasen, N.; Kern, K. *ACS Nano* **2009**, *3*, 2901–2910.
- (4) Deng, Z.; Thontasen, N.; Malinowski, N.; Rinke, G.; Harnau, L.; Rauschenbach, S.; Kern, K. *Nano Lett.* **2012**, *12*, 2452–2458.
- (5) Hamann, C.; Woltmann, R.; Hong, I.-P.; Hauptmann, N.; Karan, S.; Berndt, R. *Rev. Sci. Instrum.* **2011**, *82*, 033903.
- (6) Laskin, J.; Wang, P.; Hadjar, O. *J. Phys. Chem. C* **2010**, *114*, 5305–5311.
- (7) Johnson, G. E.; Laskin, J. *Chem. - Eur. J.* **2010**, *16*, 14433–14438.
- (8) Thontasen, N.; Levita, G.; Malinowski, N.; Deng, Z.; Rauschenbach, S.; Kern, K. *J. Phys. Chem. C* **2010**, *114*, 17768–17772.
- (9) Kley, C. S.; Dette, C.; Rinke, G.; Patrick, C. E.; Cechal, J.; Jung, S. J.; Baur, M.; Dürr, M.; Rauschenbach, S.; Giustino, F.; Stephanow, S.; Kern, K. *Nano Lett.* **2014**, *14*, 563–569.
- (10) Kondratuk, D.; Perdigão, L.; Esmail, A.; O’Shea, J. N.; Beton, P.; Anderson, H. *Nat. Chem.* **2015**, *7*, 317–322.
- (11) (a) Pauly, M.; Sroka, M.; Reiss, J.; Rinke, G.; Albarghash, A.; Vogelgesang, R.; Hahne, H.; Kuster, B.; Sesterhenn, J.; Kern, K.; Rauschenbach, S. *Analyst* **2014**, *139*, 1856–1867. (b) Gunaratne, K.; Prabhakaran, V.; Ibrahim, Y.; Norheim, R.; Johnson, G.; Laskin, J. *Analyst* **2015**, *140*, 2957–2963.
- (12) Ulas, S.; Bundschuh, S.; Jester, S.-S.; Eberl, C.; Kraft, O.; Hölscher, H.; Böttcher, A.; Kappes, M. M. *Carbon* **2014**, *68*, 125–137.
- (13) Ulas, S.; Weippert, J.; Amsharov, K.; Jansen, M.; Pop, M.; Diudea, M.; Strelnikov, D.; Böttcher, A.; Kappes, M. M. *J. Phys. Chem. C* **2015**, *119*, 7308–7318.
- (14) See for example Forney, D.; Jakobi, M.; Maier, J. P. *J. Chem. Phys.* **1989**, *90*, 600–601. Sabo, M. S.; Allison, J.; Gilbert, J. R.; Leroi, G. E. *Appl. Spectrosc.* **1991**, *45*, 535–542.
- (15) See for example Hallam, H. E., Ed.; *Vibrational Spectroscopy of Trapped Species*; John Wiley & Sons: New York, 1973. Bondybey, V. E.; English, J. H.; Miller, T. A. *J. Am. Chem. Soc.* **1978**, *100*, 5251–5252. Bondybey, V. E.; Räsänen, M.; Lammers, A. *Annu. Rep. Prog. Chem., Sect. C: Phys. Chem.* **1999**, *95*, 331–372. Jacox, M. E. *Chem. Phys.* **1994**, *189*, 149–170.
- (16) Shaffer, S. A.; Tang, K.; Anderson, G. A.; Prior, D. C.; Udseth, H. R.; Smith, R. D. *Rapid Commun. Mass Spectrom.* **1997**, *11*, 1813–1817.
- (17) Greisch, J.-F.; Harding, M. E.; Schäfer, B.; Ruben, M.; Klopfer, W.; Kappes, M. W.; Schooss, D. *J. Phys. Chem. Lett.* **2014**, *5*, 1727–1731.
- (18) Kern, B.; Strelnikov, D.; Weis, P.; Böttcher, A.; Kappes, M. M. *J. Phys. Chem. A* **2013**, *117*, 8251–8255.
- (19) Godbout, J. T.; Halasinski, T. M.; Leroi, G. E.; Allison, J. J. *J. Phys. Chem.* **1996**, *100*, 2892–2899.
- (20) Kordel, M.; Schooss, D.; Neiss, C.; Walter, L.; Kappes, M. M. *J. Phys. Chem. A* **2010**, *114*, 5509–5514.
- (21) Greisch, J.-F.; Harding, M. E.; Schäfer, B.; Rotter, M.; Ruben, M.; Klopfer, W.; Kappes, M. M.; Schooss, D. *J. Phys. Chem. A* **2014**, *118*, 94–102.
- (22) Bondybey, V.; Haddon, R.; English, J. J. *Chem. Phys.* **1984**, *80*, 5432–5437.
- (23) Kern, B.; Greisch, J.-F.; Strelnikov, D.; Schooss, D.; Ruben, M.; Schäfer, B.; Harding, M.; Klopfer, W.; Kappes, M. M. *in preparation*.
- (24) Greisch, J.-F.; Chmela, J.; Harding, M. E.; Klopfer, W.; Kappes, M. M.; Schooss, D. *in preparation*.
- (25) Kirby, A. F.; Foster, D.; Richardson, F. S. *Chem. Phys. Lett.* **1983**, *95*, 507–512.
- (26) Chaudhary, A.; van Amerom, F.; Short, R. *Rev. Sci. Instrum.* **2014**, *85*, 105101.
- (27) (a) Ludwig, R. M.; Moore, D. T. *J. Phys. Chem. Lett.* **2014**, *5*, 2947–2950. (b) Ludwig, R. M.; Moore, D. T. *J. Chem. Phys.* **2013**, *139*, 244202–1–9.
- (28) Vonderach, M.; Ehrler, O.; Weis, P.; Kappes, M. M. *Anal. Chem.* **2011**, *83*, 1108–1115.